USING SMALL MOLECULES TO TURN AN RNA APTAMER INTO SENSORS FOR INORGANIC TARGETS WITHOUT IN VITRO SELECTION

Tushar Aggarwal[1], Liming Wang[1], Bryan Gutierrez[1], Huseyin Erguven[1], Hakan Guven[1], and Enver Cagri Izgu[1,2,3] *

(1) Department of Chemistry and Chemical Biology, Rutgers University, New Brunswick, NJ 08854, USA

(2) Cancer Institute of New Jersey, Rutgers University, New Brunswick, NJ 08901, USA

(3) Rutgers Center for Lipid Research, New Jersey Institute for Food, Nutrition, and Health, Rutgers University, New Brunswick, NJ 08901, USA

*Corresponding authors: Izgu, E. C. (ec.izgu@rutgers.edu)

ABSTRACT

Fluorescent light-up aptamer (FLAP) systems are promising biosensing platforms that can be genetically encoded. Most biologically relevant inorganic molecules lack fluorogenicity or affinity for an aptamer that binds a particular organic molecule ligand. Not surprisingly, a FLAP system that can detect an inorganic molecule has yet to be developed. Here we describe a small-molecule based approach that allows for a single aptamer system with a consensus sequence known to bind a specific organic ligand to fluorogenically detect multiple, structurally unique, and non-fluorogenic inorganic targets. Guided by molecular docking and chemical functional group reactivity, we developed novel benzylidene imidazolinone architectures as pre-ligands that exhibit weak or inhibited fluorogenic binding toward Baby Spinach. These pre-ligands can be transformed into native ligands by either hydrogen sulfide (H_2S) or hydrogen peroxide (H_2O_2). Adaptation of this method to live cells through plasmid transfection opened a new opportunity for cell-based biosensing: *Escherichia coli* competent cells (BL21-DE3) transformed with a plasmid encoding Baby Spinach and incubated with the pre-ligand successfully generated fluorescence signal in response to externally introduced H_2S or H_2O_2. The reported method eliminates the need of *in vitro* selection of a new aptamer sequence for these inorganic targets, expanding the current capabilities of FLAPs. Leveraging the functional group reactivity of small molecules can lead to cell-based sensors for inorganic molecular targets, exploiting a new synergism between synthetic organic chemistry and synthetic biology.

INTRODUCTION

Aptamers are structured nucleic acid sequences that selectively bind a molecular target with high affinity. Aptamer sequences can be found in nature as gene regulation elements located in the untranslated regions of mRNAs,[1] or discovered in the laboratory by *in vitro* selection (also known as SELEX: systematic evolution of ligands by exponential enrichment) from a random pool of nucleic acids.[2,3] Some *in vitro*-selected aptamers can bind and increase the fluorescence quantum yield (Φ_F) of fluorogenic small-molecule ligands that are otherwise poorly fluorescent in their unbound state.[4,5] These aptamers, often referred to as fluorescent light-up aptamers (FLAPs),[6] have attracted significant attention due to their potential for biosensing.[7–10]

Interest in the use of FLAPs continues to evolve, yet the standard practice often requires in vitro selection of a new aptamer sequence for each new molecular target. A FLAP consensus sequence that binds a particular organic ligand molecular framework has no direct utility for detecting an inorganic target. Further, the aptamer ligand must have inherent fluorogenicity to generate fluorescence signal in a FLAP system, rendering non-fluorogenic chemical cues or biomarkers unsuitable for detection. Recent aptamer-based approaches for sensing biological inputs often involve engineering of a secondary aptamer sequence, such as a riboswitch,[11,12] that binds the input to promote conditional folding of the FLAP. However, this requires considerably long and structurally complex RNA constructs. Structure- and reactivity-guided design principles in synthetic organic chemistry can address these fundamental challenges.

Here we describe a small-molecule approach that allows for a single aptamer system with a consensus sequence known to bind a specific organic ligand to fluorogenically detect multiple, structurally unique, and non-fluorogenic inorganic targets (Figure 1). Spinach (97-nt) and its truncated version, Baby Spinach (57-nt), are RNA FLAPs that bind 4-hydroxybenzylidene imidazolinone (HBI) and various HBI analogs with a K_d in nanomolar range.[4] Guided by molecular docking and chemical functional group reactivity, we developed novel benzylidene imidazolinone (BI) architectures as caged ligands that exhibit weak or inhibited fluorogenic binding toward Baby Spinach. These BI-derived small molecules, here referred to as pre-ligands, can be transformed into native HBI ligands by a specific inorganic target. In this proof-of-concept study, we focused on redox-active inorganics: hydrogen sulfide (H_2S) and hydrogen peroxide (H_2O_2). H_2S is a reducing agent that has cytoprotective properties against oxidative stress[13] and is involved in signal transduction pathways pertaining to neurological[14–17] and cardiovascular[18,19] processes. H_2S can diffuse through lipid membranes without specialized channels.[20] H_2O_2 is an aerobic metabolite primarily generated from superoxide radical ($O_2^{\bullet -}$) by superoxide dismutases and serves as an oxidant.[21] It is involved in a number of biological processes, including signal transduction,[22,23] cell differentiation and proliferation,[24] immune response,[25] mitochondrial dysfunction,[23] and oncogene activity.[Error! Bookmark not

defined.[24,26] H_2O_2 transport across membranes occurs through simple diffusion or is facilitated by aquaporins.[27,28]

The FLAP system devised from Baby Spinach and pre-ligands can detect H_2S and H_2O_2 with good selectivity against other redox species. Adaptation of this method to live cells through plasmid transfection opened a new opportunity for cell-based biosensing: *Escherichia coli* competent cells (BL21-DE3) transformed with a Baby Spinach-encoding plasmid and incubated with the pre-ligand successfully generated fluorescence signal in response to externally introduced H_2S or H_2O_2. The reported method eliminates the need of *in vitro* selection of a new aptamer consensus sequence for each inorganic target, thereby significantly expanding the current capabilities of aptamers in the context of nucleic acid-based detection. Leveraging the functional group reactivity of small molecules can lead to cell-based sensors for inorganic molecular targets, exploiting a new synergism between synthetic organic chemistry and synthetic biology.

RESULTS AND DISCUSSION

To structurally rationalize the effect of ligand derivatization on Spinach binding, we performed docking simulations using Auto-dock Vina 1.2.0,[29,30] which presents a success rate of >90% in detecting receptor-ligand bindings with an average RMSD of <2.0 Å.[31] Recognizing the limitation of Auto-dock Vina for heteroatoms, we used methoxycarbonyl, phenyl, benzyl, and benzoyl substituents to mimic a list of representative 4-*O* caging groups (Figure 2). Based on the crystal structure of the Spinach-DFHBI complex, DFHBI forms key hydrogen bond interactions with G26/G31/A64 nucleobases in binding pocket[32] (Figure 2A). These H-bonds (four in total) were largely retained with similar bond distances after docking simulation with DFHBI (Figure 2B, docking score of -8.9 kcal mol^{-1}), validating that the native ligand-aptamer binding interactions can be attained in silico using AutoDock Vina. Strikingly, when the 4-*O* atom of DFHBI was connected to methoxycarbonyl, phenyl, benzyl, or benzoyl group, the resulting DFHBI derivative bound G26/G31/A64 with a near 180° rotation, positioning either the 4-*O*-benzylidene motif opposite to G26 (for methylcarbonyl-DFHBI, benzoyl-DFHBI, and benzyl DFHBI) or the imidazolinone carbonyl opposite to G31 (for phenyl-DFHBI). For all these derivatives, the native H-bonding interactions within the G26/G31/A64 pocket were abolished and the docking scores (methylcarbonyl-DFHBI: -5.6, phenyl-DFHBI: 2.7, benzoyl-DFHBI: -5.6, and Benzyl-DFHBI: -6.6 kcal mol^{-1}) indicated significantly weaker binding affinity. Taken together, these docking results provided support for a scenario in which the positioning of the benzylidene imidazolinone motif within the G26/G31/A64 binding pocket of Spinach can be altered by modifying the 4-*O*-benzylidene atom with a range of functional groups.

Redox-mediated chemical transformations of functional groups have been successfully implemented to release phenols.[33,34] Guided by these transformations and in agreement with the basic

functional group attachment to DFHBI in our docking simulations, we developed a library of small molecules to serve as the aptamer pre-ligands (Figure 3). This library included the pre-ligands designed to react with **(1)** H_2S: Azidoethylcarbonyl-modified MFHBI (AEC-MFHBI) and DFHBI (AEC-DFHBI); dinitrophenyl-modified MFHBI (DNP-MFHBI); pyridyldisulfunylbenzoyl-modified MFHBI (PyDSBz-MFHBI) and DBrHBI (PyDSBz-DBrHBI), or **(2)** H_2O_2: 4-(methyl)benzeneboronic acid pinacol ester-modified MFHBI (MBBAPE-MFHBI) and DFHBI (MBBAPE-DFHBI); and 4-(methyl)benzeneboronic acid-modified MFHBI (MBBA-MFHBI).

AEC-MFHBI and AEC-DFHBI displayed poor selectivity against biologically relevant thiols other than H_2S. In particular, cysteine led to a higher F/F_0 than H_2S. DNP-MFHBI and PyDSBz-MFHBI provided similar F/F_0 values for all the tested thiols. We hypothesized that the dinitrobenzyl moiety in DNP-MFHBI and the ester in PyDSBz-MFHBI may readily react with thiols and, thus, incorporation of the second fluorine atom onto the benzylidene ring would render these functional groups even more reactive. As a result, we elected to exclude the synthesis of their DFHBI analogs. For the pre-ligands designed to react with H_2O_2, both MBBAPE-MFHBI and MBBAPE-DFHBI displayed poor stability in near-neutral buffer and without H_2O_2. We observed conversion to DFHBI by MS, and their mixtures with Baby Spinach exhibited increasing levels of fluorescence, suggesting that these DFHBI-derived compounds are too reactive for assays in vitro. In contrast, the monofluoro analog MBBA-MFHBI is stable in buffer. Its DFHBI analog was not included into the library due to difficulties in synthesis and isolation. Furthermore, our preliminary findings with the HBI derivatives indicated that the solubility of boronic acid-caged pre-ligand is superior to its boronic acid pinacol ester counterpart. Based on these results, we thus conducted H_2O_2 detection experiments using MBBA-MFHBI. Furthermore, we determined the pK_a of DBrHBI as 5.2 (Figure S1) and MFHBI as 6.8 (Figure S2) using spectrophotometric methods.

Next, we evaluated the cell-free performance of the two well-performing pre-ligands PyDSBz-DBrHBI and MBBA-MFHBI for sensing H_2S and H_2O_2, respectively, via microplate reader measurements (Figure 4). For these experiments we used Baby Spinach,[32] a truncated (51-nt) version of Spinach, which can be readily obtained from either cell-free transcription or solid phase synthesis. Changes in fluorescence intensities after 60 min of incubation of a selected pre-ligand (5 μM) with Baby Spinach (1 μM) were calculated based on the signal-to-background ratio F/F_0, where F and F_0 were defined as the fluorescence with and without the analyte after 1 hour. Mammalian cells have been shown to respond to 10–600 μM H_2S as an exogenous source,[35] therefore, we reasoned that addition of Na_2S at 500 μM into a buffer at pH 7.4 can serve as a proper mimic for biological H_2S environment. At neutral pH, around 20% of its sulfur containing forms should exist as H_2S (~100 μM), based on the pK_a (~6.9) of NaSH.[36] Results indicated that PyDSBz-DBrHBI achieved an F/F_0 of 37.3 with 500 μM Na_2S as the source of H_2S, indicating an increase in fluorescence ~3600%. We also recorded the fluorescence intensities every 10 minutes over

a 60-minute incubation period and compared them with those of Baby Spinach with DBrHBI (Figure 4A). Fluorescence intensities of samples containing PyDSBz-DBrHBI plateaued at ~50 minutes and reached up to ~30% of that with DBrHBI. To assess the performance of the H_2O_2-responsive pre-ligand, MBBA-MFHBI, we monitored the relative fluorescence intensity change of Baby Spinach solution containing either MFHBI or MBBA-MFHBI in presence of H_2O_2 over 60 minutes (Figure 4D). After the addition of H_2O_2 (estimated concentration of 100 μM upon mixing) to the solution containing MBBA-MFHBI, we observed ~2500% increase in fluorescence intensity (F/F_0 = 25.2) compared to only 28% increase without H_2O_2 addition, suggesting that phenyl boronic acid group of MBBA-MFHBI is stable at physiological pH and can generate free MFHBI upon reacting with H_2O_2. Fluorescence intensities of MBBA-MFHBI in the presence of H_2O_2 reached up to ~75% that of MFHBI within 1 hour.

We then conducted a fluorescence quenching assay to gain an understanding of relative fluorogenic binding affinities of these pre-ligands compared to their native counterparts. Toward this goal, we incubated a constant concentration of the active ligand (2 μM) with varied concentrations of the pre-ligand, together with 1 μM of Baby Spinach, and the fluorescence intensities were recorded after 1 hour of incubation. Samples containing 50 μM PyDSBz-DBrHBI presented similar fluorescence signals to those of 0 μM, which represented minimal competition between PyDSBz-DBrHBI and DBrHBI (Figure S3). Incubating 50 μM MBBA-MFHBI with 2 μM MFHBI still showed a retain of fluorescence at 69.8% compared to samples without any pre-ligand (Figure S4), meaning the binding of MBBA-MFHBI towards Baby Spinach is much weaker than the binding between MFHBI and Baby Spinach. These results correlate well with the predicted weaker binding of pre-ligands to Spinach from the docking simulations.

Next, we evaluated the redox-specificities of the aptamer pre-ligands PyDSBz-DBrHBI (Figures 4B) and MBBA-MFHBI (Figures 4E). The fluorescence intensities were recorded after incubating a mixture of the pre-ligand and Baby Spinach with a redox agent for 1 hour, and F/F_0 were calculated, where F and F_0 are the fluorescence intensities for samples with and without the redox agents, respectively. The F/F_0 value for the control samples, which included only the pre-ligand and Baby Spinach in buffer, were set to 1 for comparison. For a mixture of PyDSBz-DBrHBI and Baby Spinach was incubated with Na_2S (500 μM) for 1 hour, F/F_0 was measured as 37.3. Of significant note, when the same mixture was incubated with cysteine and glutathione, which are nucleophilic thiols abundant in biological environments, F/F_0 reached just 6.6 and 3.9, respectively. Other RSS we tested (Cysteine, Glutathione, SO_3^{2-}, $S_2O_3^{2-}$, SO_4^{2-}, and SCN^-) generated F/F_0 values centered around ~1, indicating no measurable pre-ligand activation. As for the samples containing MBBA-MFHBI, F/F_0 was 25.2 with H_2O_2 after 1 hour of incubation. In contrast, F/F_0 values were <4 for other ROS ($^{\bullet}NO$, $^1O_2$, $O_2^{-\bullet}$, $^{\bullet}OH$ and H_2S), suggesting that MBBA-MFHBI is selective for H_2O_2.

Limit of detection (LoD) values were determined for pre-ligands PyDSBz-DBrHBI and MBBA-MFHBI by evaluating the statistical difference between F and F_0 measured with Baby Spinach at different concentrations of H_2S and H_2O_2, respectively (Figures 4C and 4F). Here, LoD is defined as the minimum redox agent concentration at which F is statistically higher than F_0 according to the one-tailed Student's t test. We determined LoD for PyDSBz-DBrHBI as 0.2 μM of H_2S and that for MBBA-MFHBI as 0.2 μM of H_2O_2. The LoD of PyDSBz-DBrHBI determined is close to other recently reported fluorescence-based H_2S sensing systems.[37–39] The sensitivity of MBBA-MFHBI is comparable to fluorescence-based H_2O_2 sensors that use small-molecule fluorophore activation.[40,41]

We first transformed chemically competent *E. coli* BL21 Star (DE3) with a DNA plasmid containing a single tRNA-Spinach2 construct.[42] Confocal imaging of these *E. coli* in the presence of MFHBI exhibited weak brightness at 488 nm excitation. In order to achieve higher intensity fluorescence outputs, we designed and cloned an aptamer with tRNA followed by three continual Baby Spinach consensus regions, each connected through a 6-bp-long sealing stem (named pET-21-3xBaby Spinach, Figures S5 and S6). A similar construct was successfully demonstrated to increase fluorescence intensity *in vitro*.[43] In line with this observation, we reasoned that *E. coli* transcribing our pET-21-3xBaby Spinach construct would, therefore, generate more copies of DBrHBI or MFHBI binding sites compared to the single tRNA-Spinach2 construct and, thus, could generate stronger fluorescence signal when exposed to H_2S or H_2O_2 under same conditions. Indeed, we observed satisfactorily bright signals in samples incubated with DBrHBI at 440 nm excitation (Figure 4A, left) and MFHBI at 488 nm excitation (Figure 4C, left). For these positive controls and subsequent experiments, *E. coli.* carrying our custom designed pET-21-3xBaby Spinach plasmid were grown in LB at 37 °C. RNA transcription was induced by the addition of 1 mM isopropyl β-D-1-thiogalactopyranoside (IPTG) once OD (600) reached 0.4, and cells were allowed to grow for an additional 2 hours to facilitate aptamer transcription. Harvested cells were incubated with M9 media containing either PyDSBz-DBrHBI (100 μM) or MBBA-MFHBI (100 μM) for 15 min. The media was replaced with fresh media containing either H_2O_2 (100 μM) or Na_2S (2 mM). Aliquots (1 mL) of *E. coli.* culture were taken at different time points for confocal imaging, for which a red membrane dye (Fm 4-64FX) was used as a co-stain to label the *E. coli* membrane. It is worth noting that the use of Fm 4-64FX allowed us to observe heterogeneity in the overall population for aptamer transcription levels, as the positive control cells (Figures 4A and 4C, left) displayed different levels of brightness following excitation at either 440 nm or 488 nm.

Samples without DBrHBI (Figure 4A, middle) or MFHBI (Figure 4C, middle) served as a measure of background fluorescence, and subsequent confocal images were adjusted based on the parameters acquired during these control experiments and data analyses. *E. coli.* samples carrying the control vector

plasmid pUC19, which contained no 3xBaby Spinach aptamer gene, exhibited no detectable fluorescence in the presence of either DBrHBI (Figure 4A, right) or MFHBI (Figure 4C, right). With *E. coli.* samples incubated with PyDSBz-DBrHBI (100 μM), where Na_2S (2mM) was introduced exogenously, we observed a gradual increase in fluorescent cell population over time (Figure 4B). Notably, single cell fluorescence output plateaus within 30 min. We observed a similar trend of increase in fluorescence output from *E. coli* containing MBBA-MFHBI (100 μM) and incubated with exogenous H_2O_2 (100 μM) (Figure 4D). Fluorescence signals from *E. coli* were detected within 15 minutes upon addition of H_2O_2. We observed insignificant changes in single cell fluorescence for samples imaged at 30 and 60 minutes of incubation.

CONCLUSION

Aptamer-based detection of molecular targets have emerged as promising biosensing tools that can be genetically encoded. Interest in the use of FLAPs continues to evolve, yet the standard practice requires in vitro selection of a new aptamer for each new molecular target or inclusion of a secondary aptamer sequence to promote the folding of the FLAP sequence. Even though these approaches find biological use for a particular target, there has been no report on the design of a single aptamer that can be purposed for multiple, structurally distinct targets. In addition, to our best knowledge, there is no available FLAP system that can detect inorganic redox species, such as reactive oxygen or sulfur species. Structure- and reactivity-guided design principles in synthetic organic chemistry can address these fundamental challenges. In this work, we developed a library of small molecules to serve as aptamer pre-ligands, based on their redox-reactive functional group modifications. Specifically, a FLAP system composed of Baby Spinach and PyDSBz-DBrHBI or MBBA-MFHBI exhibited significant levels of fluorescence enhancement in the presence of H_2S or H_2O_2. This approach was successfully implemented in *E. coli*, which served as cell-based sensors for these redox species. Our study shows the potential of synthetic organic chemistry in expanding the applications of aptamers beyond their traditional roles in synthetic biology and biosensing.

ACKNOWLEDGMENTS

We thank Edward W. Castner, Advaitha Madireddy, George Giambasu, Alec Meacham, Robert Puhak, Kern Hast and Jonathan Hong for useful discussions. We acknowledge Magali Rhia L. Stone for guidance in microscopy sample preparation. We acknowledge the Office of Advanced Research Computing (OARC) at Rutgers for providing access to the Amarel cluster. This work was supported by the US National Institutes of Health / National Institute of Biomedical Imaging and Bioengineering, Trailblazer Award (EB029548), the American Cancer Society, Institutional Research Grant Early Investigator Award, and the Rutgers Cancer Institute of New Jersey NCI Cancer Center Support Grant (P30CA072720), and Busch Biomedical Grant (to E.C.I.); and Steven A. Cox Scholarship for Cancer Research (to T.A.).

AUTHOR CONTRIBUTIONS

E.C.I. conceived the study. T.A. conducted molecular docking, plasmid design, molecular biology experiments, and microscopy. L.W., B.G., H.E., and H.G. conducted the pre-ligand syntheses, spectroscopic and spectrophotometric characterizations. All of the authors contributed to the interpretation of data. T.A., L.W., and E.C.I. wrote the manuscript with input from other authors. E.C.I. supervised the study.

DECLARATION OF INTEREST

E.C.I. and T.A. are co-inventors of a patent application filed by Rutgers University on the subject of this work.

REFERENCES

(1) Roth, A.; Breaker, R. R. The Structural and Functional Diversity of Metabolite-Binding Riboswitches. *Annu. Rev. Biochem.* **2009**, *78* (1), 305–334. https://doi.org/10.1146/annurev.biochem.78.070507.135656.

(2) Ellington, A. D.; Szostak, J. W. In Vitro Selection of RNA Molecules That Bind Specific Ligands. *Nature* **1990**, *346* (6287), 818–822. https://doi.org/10.1038/346818a0.

(3) Tuerk, C.; Gold, L. Systematic Evolution of Ligands by Exponential Enrichment: RNA Ligands to Bacteriophage T4 DNA Polymerase. *Science* **1990**, *249* (4968), 505–510. https://doi.org/10.1126/science.2200121.

(4) Paige, J. S.; Wu, K. Y.; Jaffrey, S. R. RNA Mimics of Green Fluorescent Protein. *Science* **2011**, *333* (6042), 642–646. https://doi.org/10.1126/science.1207339.

(5) Babendure, J. R.; Adams, S. R.; Tsien, R. Y. Aptamers Switch on Fluorescence of Triphenylmethane Dyes. *J. Am. Chem. Soc.* **2003**, *125* (48), 14716–14717. https://doi.org/10.1021/ja037994o.

(6) Neubacher, S.; Hennig, S. RNA Structure and Cellular Applications of Fluorescent Light-Up Aptamers. *Angew. Chem. Int. Ed.* **2019**, *58* (5), 1266–1279. https://doi.org/10.1002/anie.201806482.

(7) Montagud-Martínez, R.; Heras-Hernández, M.; Goiriz, L.; Daròs, J.-A.; Rodrigo, G. CRISPR-Mediated Strand Displacement Logic Circuits with Toehold-Free DNA. *ACS Synth. Biol.* **2021**, *10* (5), 950–956. https://doi.org/10.1021/acssynbio.0c00649.

(8) Khan, P.; Aufdembrink, L. M.; Engelhart, A. E. Isothermal SARS-CoV-2 Diagnostics: Tools for Enabling Distributed Pandemic Testing as a Means of Supporting Safe Reopenings. *ACS Synth. Biol.* **2020**, *9* (11), 2861–2880. https://doi.org/10.1021/acssynbio.0c00359.

(9) Liu, X.; Wang, T.; Wu, Y.; Tan, Y.; Jiang, T.; Li, K.; Lou, B.; Chen, L.; Liu, Y.; Liu, Z. Aptamer Based Probes for Living Cell Intracellular Molecules Detection. *Biosens. Bioelectron.* **2022**, *208*, 114231. https://doi.org/10.1016/j.bios.2022.114231.

(10) Zhao, Y.; Ong, S.; Chen, Y.; Huang, P.-J. J.; Liu, J. Label-Free and Dye-Free Fluorescent Sensing of Tetracyclines Using a Capture-Selected DNA Aptamer. *Anal. Chem.* **2022**, *94* (28), 10175–10182. https://doi.org/10.1021/acs.analchem.2c01561.

(11) Sun, Z.; Wu, R.; Zhao, B.; Zeinert, R.; Chien, P.; You, M. Live-Cell Imaging of Guanosine Tetra- and Pentaphosphate (p)PpGpp with RNA-based Fluorescent Sensors**. *Angew. Chem. Int. Ed.* **2021**, *60* (45), 24070–24074. https://doi.org/10.1002/anie.202111170.

(12) You, M.; Litke, J. L.; Jaffrey, S. R. Imaging Metabolite Dynamics in Living Cells Using a Spinach-Based Riboswitch. *Proc. Natl. Acad. Sci.* **2015**, *112* (21), E2756–E2765. https://doi.org/10.1073/pnas.1504354112.

(13) Olas, B. Hydrogen Sulfide as a “Double-Faced” Compound: One with Pro- and Antioxidant Effect. *Adv. Clin. Chem.* **2016**, *78*, 187–196. https://doi.org/10.1016/bs.acc.2016.07.005.

(14) Kimura, H. Hydrogen Sulfide Induces Cyclic AMP and Modulates the NMDA Receptor. *Biochem. Biophys. Res. Commun.* **2000**, *267* (1), 129–133. https://doi.org/10.1006/bbrc.1999.1915.

(15) Han, Y.; Qin, J.; Chang, X.; Yang, Z.; Bu, D.; Du, J. Modulating Effect of Hydrogen Sulfide on Gamma-Aminobutyric Acid B Receptor in Recurrent Febrile Seizures in Rats. *Neurosci. Res.* **2005**, *53* (2), 216–219. https://doi.org/10.1016/j.neures.2005.07.002.

(16) Sun, W.-H.; Liu, F.; Chen, Y.; Zhu, Y.-C. Hydrogen Sulfide Decreases the Levels of ROS by Inhibiting Mitochondrial Complex IV and Increasing SOD Activities in Cardiomyocytes under Ischemia/Reperfusion. *Biochem. Biophys. Res. Commun.* **2012**, *421* (2), 164–169. https://doi.org/10.1016/j.bbrc.2012.03.121.

(17) Kimura, Y.; Goto, Y.-I.; Kimura, H. Hydrogen Sulfide Increases Glutathione Production and Suppresses Oxidative Stress in Mitochondria. *Antioxid. Redox Signal.* **2010**, *12* (1), 1–13. https://doi.org/10.1089/ars.2008.2282.

(18) Lefer, D. J. A New Gaseous Signaling Molecule Emerges: Cardioprotective Role of Hydrogen Sulfide. *Proc. Natl. Acad. Sci.* **2007**, *104* (46), 17907–17908. https://doi.org/10.1073/pnas.0709010104.

(19) Polhemus, D. J.; Lefer, D. J. Emergence of Hydrogen Sulfide as an Endogenous Gaseous Signaling Molecule in Cardiovascular Disease. *Circ. Res.* **2014**, *114* (4), 730–737. https://doi.org/10.1161/circresaha.114.300505.

(20) Mathai, J. C.; Missner, A.; Kügler, P.; Saparov, S. M.; Zeidel, M. L.; Lee, J. K.; Pohl, P. No Facilitator Required for Membrane Transport of Hydrogen Sulfide. *Proc. Natl. Acad. Sci.* **2009**, *106* (39), 16633–16638. https://doi.org/10.1073/pnas.0902952106.

(21) D'Autréaux, B.; Toledano, M. B. ROS as Signalling Molecules: Mechanisms That Generate Specificity in ROS Homeostasis. *Nat. Rev. Mol. Cell Biol.* **2007**, *8* (10), 813–824. https://doi.org/10.1038/nrm2256.

(22) Sies, H.; Jones, D. P. Reactive Oxygen Species (ROS) as Pleiotropic Physiological Signalling Agents. *Nat. Rev. Mol. Cell Biol.* **2020**, *21* (7), 363–383. https://doi.org/10.1038/s41580-020-0230-3.

(23) Sies, H. Role of Metabolic H2O2 Generation REDOX SIGNALING AND OXIDATIVE STRESS*. *J. Biol. Chem.* **2014**, *289* (13), 8735–8741. https://doi.org/10.1074/jbc.r113.544635.

(24) Lennicke, C.; Rahn, J.; Lichtenfels, R.; Wessjohann, L. A.; Seliger, B. Hydrogen Peroxide – Production, Fate and Role in Redox Signaling of Tumor Cells. *Cell Commun. Signal. : CCS* **2015**, *13* (1), 39. https://doi.org/10.1186/s12964-015-0118-6.

(25) Cordeiro, J. V.; Jacinto, A. The Role of Transcription-Independent Damage Signals in the Initiation of Epithelial Wound Healing. *Nat. Rev. Mol. Cell Biol.* **2013**, *14* (4), 249–262. https://doi.org/10.1038/nrm3541.

(26) Cheung, E. C.; Vousden, K. H. The Role of ROS in Tumour Development and Progression. *Nat. Rev. Cancer* **2022**, *22* (5), 280–297. https://doi.org/10.1038/s41568-021-00435-0.

(27) Bienert, G. P.; Møller, A. L. B.; Kristiansen, K. A.; Schulz, A.; Møller, I. M.; Schjoerring, J. K.; Jahn, T. P. Specific Aquaporins Facilitate the Diffusion of Hydrogen Peroxide across Membranes*. *J. Biol. Chem.* **2007**, *282* (2), 1183–1192. https://doi.org/10.1074/jbc.m603761200.

(28) Bienert, G. P.; Desguin, B.; Chaumont, F.; Hols, P. Channel-Mediated Lactic Acid Transport: A Novel Function for Aquaglyceroporins in Bacteria. *Biochem. J.* **2013**, *454* (3), 559–570. https://doi.org/10.1042/bj20130388.

(29) Trott, O.; Olson, A. J. AutoDock Vina: Improving the Speed and Accuracy of Docking with a New Scoring Function, Efficient Optimization, and Multithreading. *J. Comput. Chem.* **2010**, *31* (2), 455–461. https://doi.org/10.1002/jcc.21334.

(30) Eberhardt, J.; Santos-Martins, D.; Tillack, A. F.; Forli, S. AutoDock Vina 1.2.0: New Docking Methods, Expanded Force Field, and Python Bindings. *J. Chem. Inf. Model.* **2021**, *61* (8), 3891–3898. https://doi.org/10.1021/acs.jcim.1c00203.

(31) Su, M.; Yang, Q.; Du, Y.; Feng, G.; Liu, Z.; Li, Y.; Wang, R. Comparative Assessment of Scoring Functions: The CASF-2016 Update. *J. Chem. Inf. Model.* **2019**, *59* (2), 895–913. https://doi.org/10.1021/acs.jcim.8b00545.

(32) Warner, K. D.; Chen, M. C.; Song, W.; Strack, R. L.; Thorn, A.; Jaffrey, S. R.; Ferré-D'Amaré, A. R. Structural Basis for Activity of Highly Efficient RNA Mimics of Green Fluorescent Protein. *Nat. Struct. Mol. Biol.* **2014**, *21* (8), 658–663. https://doi.org/10.1038/nsmb.2865.

(33) Wang, Z.; Li, Y.; Zhang, Q.; Jing, C.; Jiang, Y.; Yang, T.; Han, T.; Xiong, F. A Highly Selective and Easily Acquisitive Near-Infrared Fluorescent Probe for Detection and Imaging of Hydrogen Sulfide in Cells. *Spectrochim. Acta Part A: Mol. Biomol. Spectrosc.* **2023**, *293*, 122428. https://doi.org/10.1016/j.saa.2023.122428.

(34) Lin, V. S.; Chen, W.; Xian, M.; Chang, C. J. Chemical Probes for Molecular Imaging and Detection of Hydrogen Sulfide and Reactive Sulfur Species in Biological Systems. *Chem. Soc. Rev.* **2014**, *44* (14), 4596–4618. https://doi.org/10.1039/c4cs00298a.

(35) Papapetropoulos, A.; Pyriochou, A.; Altaany, Z.; Yang, G.; Marazioti, A.; Zhou, Z.; Jeschke, M. G.; Branski, L. K.; Herndon, D. N.; Wang, R.; Szabó, C. Hydrogen Sulfide Is an Endogenous Stimulator of Angiogenesis. *Proc National Acad Sci* **2009**, *106* (51), 21972–21977. https://doi.org/10.1073/pnas.0908047106.

(36) Wang, R. Physiological Implications of Hydrogen Sulfide: A Whiff Exploration That Blossomed. *Physiol Rev* **2012**, *92* (2), 791–896. https://doi.org/10.1152/physrev.00017.2011.

(37) Pose, M.; Dillon, K. M.; Denicola, A.; Alvarez, B.; Matson, J. B.; Möller, M. N.; Cuevasanta, E. Fluorescent Detection of Hydrogen Sulfide (H2S) through the Formation of Pyrene Excimers Enhances H2S Quantification in Biochemical Systems. *J. Biol. Chem.* **2022**, *298* (10), 102402. https://doi.org/10.1016/j.jbc.2022.102402.

(38) Peng, S.; Zhong, T.; Guo, T.; Shu, D.; Meng, D.; Liu, H.; Guo, D. A Novel Fluorescent Probe for Selective Detection of Hydrogen Sulfide in Living Cells. *N. J. Chem.* **2018**, *42* (7), 5185–5192. https://doi.org/10.1039/c7nj04577h.

(39) Chen, H.; Wu, X.; Yang, S.; Tian, H.; Liu, Y.; Sun, B. A Visible Colorimetric Fluorescent Probe for Hydrogen Sulfide Detection in Wine. *J. Anal. Methods Chem.* **2019**, *2019*, 2173671. https://doi.org/10.1155/2019/2173671.

(40) Bolland, H. R.; Hammond, E. M.; Sedgwick, A. C. A Fluorescent Probe Strategy for the Detection and Discrimination of Hydrogen Peroxide and Peroxynitrite in Cells. *Chem. Commun.* **2022**, *58* (76), 10699–10702. https://doi.org/10.1039/d2cc03406a.

(41) Zuo, Y.; Jiao, Y.; Ma, C.; Duan, C. A Novel Fluorescent Probe for Hydrogen Peroxide and Its Application in Bio-Imaging. *Molecules* **2021**, *26* (11), 3352. https://doi.org/10.3390/molecules26113352.

(42) Wang, X. C.; Wilson, S. C.; Hammond, M. C. Next-Generation RNA-Based Fluorescent Biosensors Enable Anaerobic Detection of Cyclic Di-GMP. *Nucleic Acids Res.* **2016**, *44* (17), e139–e139. https://doi.org/10.1093/nar/gkw580.

(43) Shechner, D. M.; Hacisuleyman, E.; Younger, S. T.; Rinn, J. L. Multiplexable, Locus-Specific Targeting of Long RNAs with CRISPR-Display. *Nat. Methods* **2015**, *12* (7), 664–670. https://doi.org/10.1038/nmeth.3433.

FIGURES

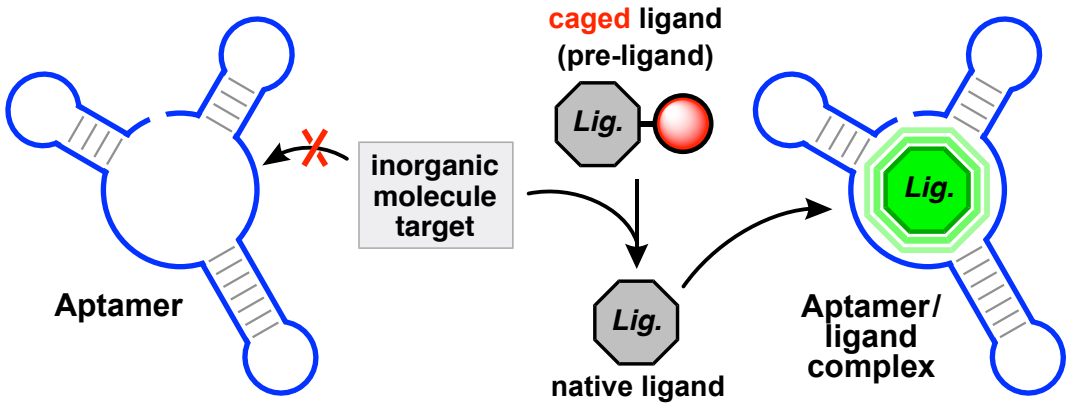

Figure 1. Conceptual illustration of how an aptamer system can detect an inorganic molecule. Here, the inorganic target has no requirement of being fluorogenic or having affinity for the aptamer. The aptamer consensus sequence binds only its native ligand but not the inorganic target. The strategy of using a caged ligand (pre-ligand) that can be converted to the native ligand by the inorganic molecule allows its detection using the aptamer.

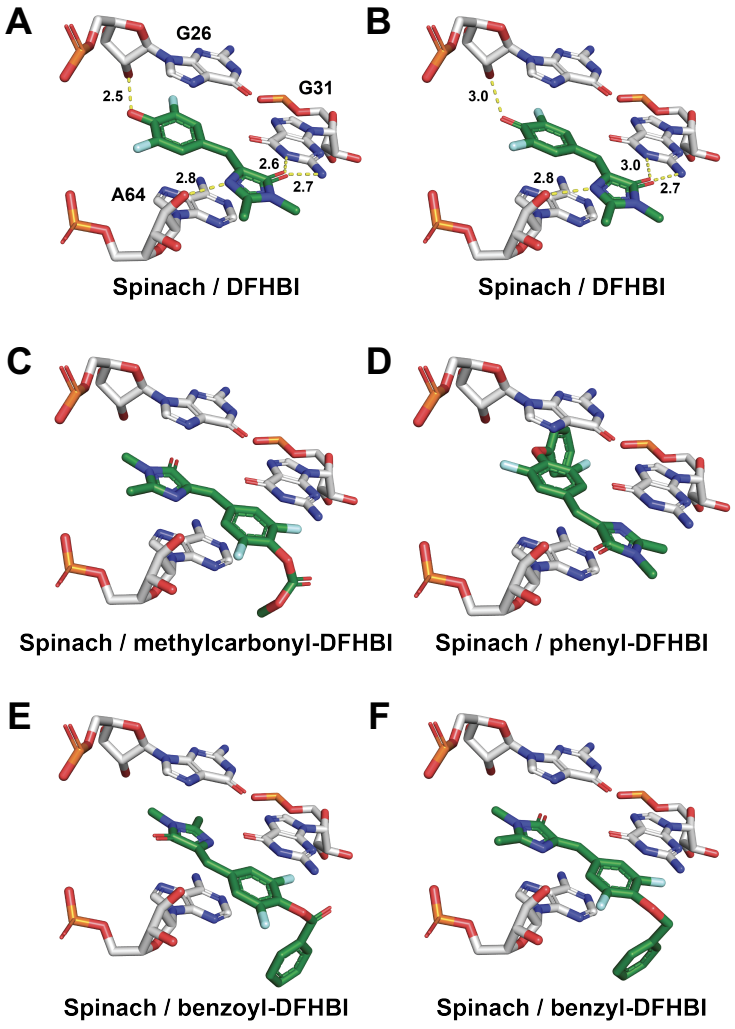

Figure 2. Docked poses: binding mode of the selected 4-*O*-aryl-caged small molecule derivatives of DFHBI. (A) Model of key hydrogen-bonding interactions within the crystal structure of Spinach-DFHBI (PDB:4TS2) near the binding site. **(B)** binding mode of the DFHBI ligand prepared in silico and docked using AutoDock Vina. **(C-F)** docked poses of the 4-*O*-aryl-caged small molecule derivatives of DFHBI.

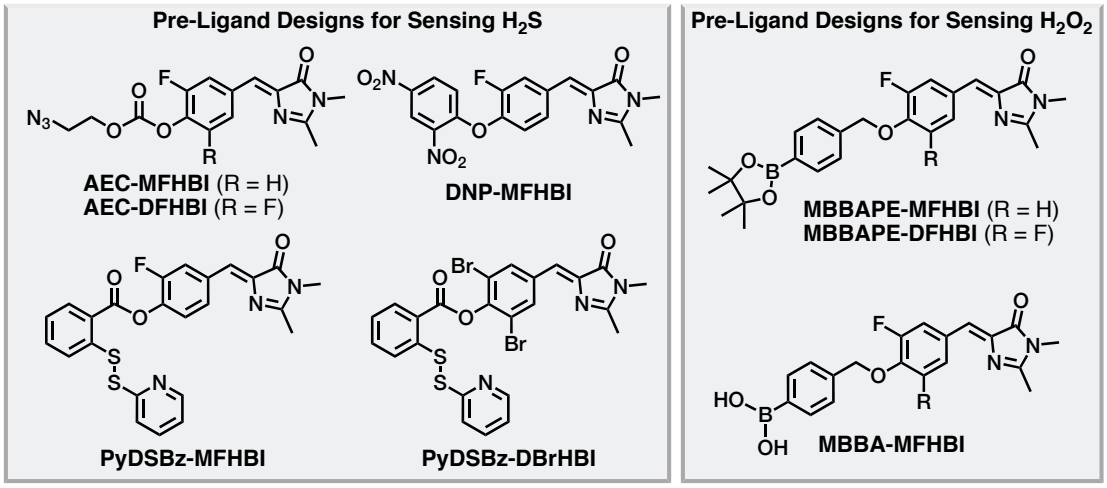

Figure 3. Aptamer pre-ligands designed to function with H_2S or H_2O_2.

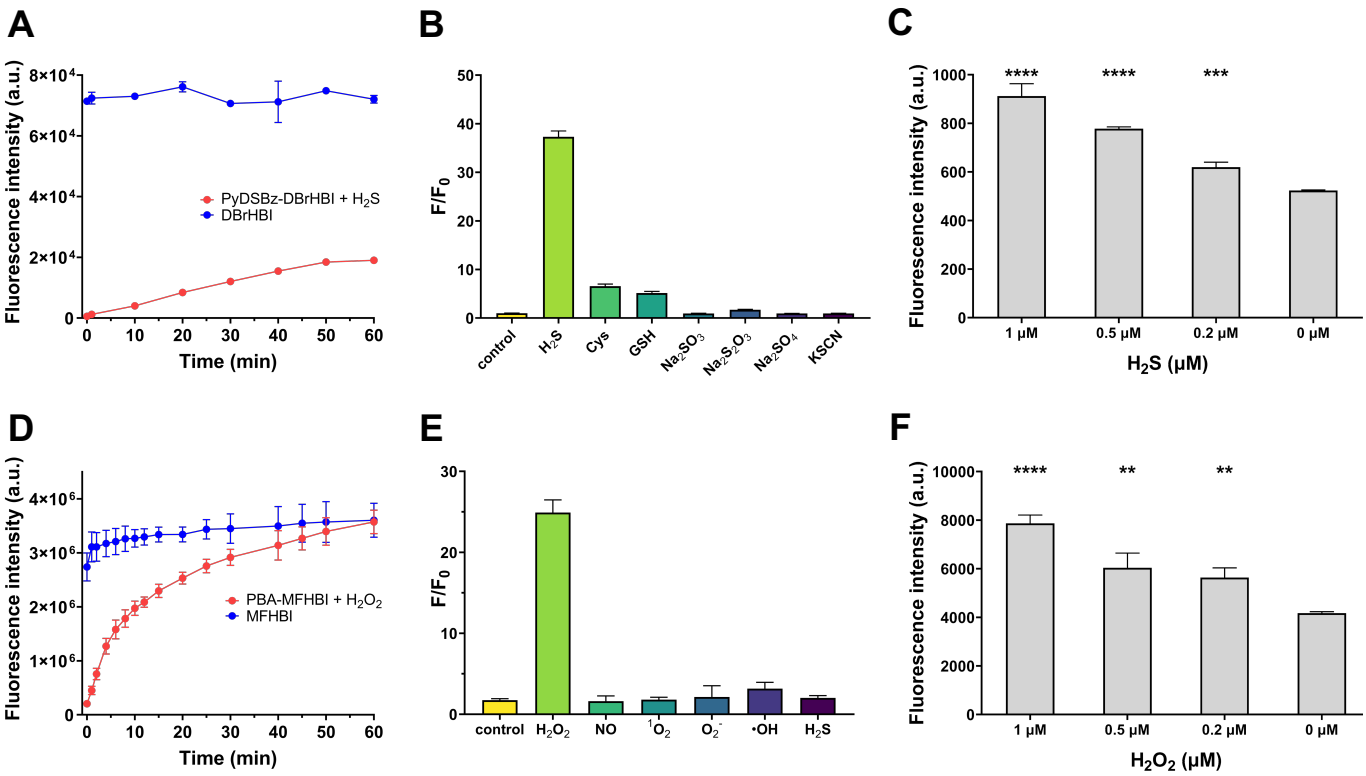

Figure 4. In vitro performance of PyDSBz-DBrHBI and MBBA-MFHBI with Baby Spinach. (A and D) Time-dependent fluorescence increase of pre-ligands upon addition of their respective redox agents (Na_2S at 500 μM, H_2O_2 at 100 μM). (B and E) The fluorescence fold increase (F/F_0) with the addition of RSS (500 μM) and ROS (100 μM), respectively. (C and F) LoD measurements for PyDSBz-DBrHBI and MBBA-MFHBI, respectively. Error bars represent standard deviation based on triplicates. Single- tailed Student's *t* test: *, P <0.05; **, P <0.01; ***, P <0.001; ****, P <0.0001. ABA- probes, MBBA-MFHBI for H_2O_2 sensing. Time-dependent change in fluorescence intensity upon addition of H_2O_2. MFHBI, and MBBA-MFHBI (5 μM), Baby Spinach (1 μM), HEPES (pH 7.4, 50 mM), KCl (100 mM), $MgCl_2$ (10 mM), and H_2O_2 (100 μM). Error bars represent standard deviation based on triplicates. Bar graph: Signal turn on (F/F_0) 60 min after addition of analyte.

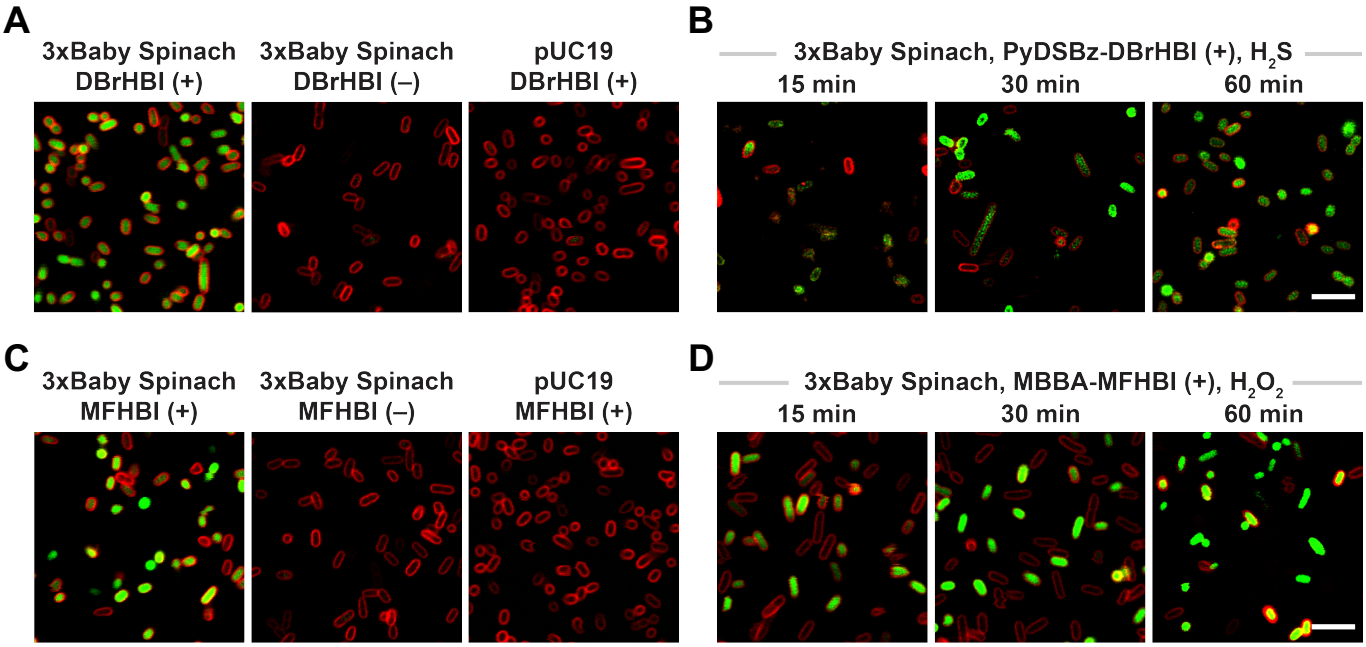

Figure 5. Confocal microscopy images of live *E. coli* for sensing (A,B) H_2S or (C,D) H_2O_2. (A) DBrHBI, (B) PyDSBz-DBrHBI, (C) MFHBI, and (D) MBBA-MFHBI activity in live *E. coli.* cells. BL21 Star (DE3) *E. coli* were transformed with either pET-21-3xBaby Spinach or pUC19 (control) plasmid. Cell were incubated in M9 media containing 100 μM of **(A)** DBrHBI, **(B)** PyDSBz-DBrHBI, **(C)** MFHBI or **(D)** MBBA-MFHBI. Redox species introduced to the imaging media: **(B)** H_2O_2 (100 μM), **(D)** Na_2S (2 mM). Upon the addition of the redox species, *E. coli* were imaged at 15, 30, and 60 minutes. For co-staining cells were treated with a FM 4-64FX (red membrane dye, 1 μg/ml, 2 min). DBrHBI channel: 440 nm excitation, MFHBI channel: 488 nm excitation, Fm4-64FX channel: 568 nm excitation. Scale bar: 5 μm.